



Thermalization of a disordered interacting system under an interaction quenchEric Dohner ¹, Hanna Terletska,² and Herbert F. Fotso ³¹*Department of Physics, University at Albany (SUNY), Albany, New York 12222, USA*²*Department of Physics and Astronomy, Middle Tennessee State University, Murfreesboro, Tennessee 37132, USA*³*Department of Physics, University at Buffalo SUNY, Buffalo, New York 14260, USA*

(Received 11 March 2023; accepted 21 September 2023; published 3 October 2023)

Although most studies of strongly correlated systems away from equilibrium have focused on clean systems, it is well known that disorder may significantly modify observed properties in various nontrivial ways. The nonequilibrium interplay of interaction and disorder in these systems thus requires further investigation. In the present paper, we use the recently developed nonequilibrium DMFT+CPA embedding scheme, that combines both the dynamical mean field theory (DMFT) and the coherent potential approximation (CPA) nonequilibrium extensions, to characterize the relaxation and the thermalization of a disordered interacting system described by the Anderson-Hubbard model under an interaction quench. The system, initially in equilibrium at a given temperature, has the interaction abruptly switched from zero to a finite value at a given time. To investigate the role of disorder, we use our effective medium approach to calculate, for different values of the final interaction and of the disorder strength, the distribution functions as the system evolves in time. This allows us to determine the effective temperature after the quench and to analyze the effects of disorder on the thermalization for various interaction strengths. We find that, for moderate interactions after the interaction quench, disorder can tune the final temperature of the system across a broad range of values with increased disorder strength leading to lower effective temperature.

DOI: [10.1103/PhysRevB.108.144202](https://doi.org/10.1103/PhysRevB.108.144202)**I. INTRODUCTION**

The dynamics of quantum systems away from equilibrium has been the subject of increased interest as a result of the recent experimental advances extending from quantum information processing platforms to time-resolved spectroscopies. A salient question that has garnered a great deal of attention is that of how quantum systems thermalize (or not) when they are abruptly driven out of equilibrium. Beyond the theoretical question of how thermalization arises in quantum systems that are supposed to be governed in their dynamics by unitary time evolution operators [1–3], these research questions have important experimental consequences. For instance, it is often typical in the analysis of pump-probe spectroscopy experiments to use a so-called “hot” electrons model whereby electrons are driven by the pump pulse into an equilibrated state that is thermalized at a higher temperature than that of the initial system [4,5]. This brings into focus the importance of the relevant relaxation scenarios and the associated timescales. Also, experiments simulating various lattice models in optical lattices are either intrinsically out of equilibrium or can be used to simulate, through their high degree of tunability, the dynamics of nonequilibrium quantum systems [6–9]. This further highlights the need for accurate modeling and benchmarking.

While numerous efforts have been dedicated to the investigation of the thermalization of correlated quantum systems away from equilibrium [10–12], little has been done to explore the effect of disorder which we can anticipate, in some circumstances, to have significant impacts on the dynamics [13–15] and which we know to be ubiquitous

in most systems of interest. In particular, nonequilibrium dynamical mean field theory (DMFT) was used to investigate the thermalization of correlated systems in a variety of nonequilibrium scenarios extending from interaction quenches [16,17], to DC field-driven systems [10,11,18–20], to simulations of time-resolved spectroscopies [21,22]. However, the effect of disorder in the thermalization of these nonequilibrium systems remains generally understudied.

In this paper we use the recently developed nonequilibrium DMFT+CPA embedding scheme [23] that combines the nonequilibrium extensions of both DMFT [10–12,24–28] and CPA (coherent potential approximation) [29–34], to investigate the thermalization dynamics of a correlated disordered system modeled by the Anderson-Hubbard model under an interaction quench. In this way, we are able to assess the impact of the disorder on the relaxation of the system and, specifically, to evaluate the temperature of the system once it has settled into its long-time thermal state. We analyze the nonequilibrium distribution functions calculated after the quench for various values of the final interaction strengths and as a function of disorder strength. We find that, for moderate interactions after the interaction quench, disorder can tune the final temperature of the system across a broad range of values with increased disorder strength leading to lower effective temperature.

The rest of the paper is structured as follows: In Sec. II, we briefly discuss the model and review the nonequilibrium DMFT+CPA formalism and its numerical implementation. In Sec. III, we present the results that describe the thermalization of the system after relaxation of the system following the

interaction quench. We end the paper with our conclusion in Sec. IV.

II. MODEL AND METHODS

A. Model

We consider a correlated disordered system described by the Anderson-Hubbard model initially in equilibrium at temperature $1/\beta$. The Hamiltonian is given by Eq. (1), where $t_{ij} = t_{\text{hop}}$ is the hopping amplitude between nearest-neighbor sites (denoted by $\langle ij \rangle$), $U(t)$ is the Coulomb interaction strength, and V_i is the random on-site disorder for site i . $c_{i\sigma}^\dagger$ and $c_{i\sigma}$ are, respectively, the creation and the annihilation operators for a particle of spin $\sigma = \uparrow, \downarrow$ at site i . $n_{i\sigma}$ is the number of particles of spin $\sigma = \uparrow, \downarrow$ at site i and μ is the chemical potential. We study the system at half-filling, such that $\mu = U/2$.

$$H = - \sum_{\langle ij \rangle \sigma} t_{ij} (c_{i\sigma}^\dagger c_{j\sigma} + \text{H.c.}) + \sum_i U(t) n_{i\uparrow} n_{i\downarrow} + \sum_{i\sigma} (V_i - \mu) n_{i\sigma}. \quad (1)$$

In equilibrium, the Coulomb interaction is constant $U(t) = U$. In the nonequilibrium scenario of interest in this work, it is given by a step function $U(t) = \Theta(t - t_{\text{quench}})U_2$ with $t_{\text{quench}} = 0$, such that the interaction is $U_1 = 0$ for negative times and some constant $U_2 \neq 0$ for positive times. The on-site disorder V_i is constant in time and follows a uniform distribution such that $P(V_i) = \frac{1}{2W} \Theta(W - |V_i|)$, where W is the disorder strength. We use the notation $\langle \dots \rangle_{\{V\}}$ to indicate averaging over all disorder values in the angle brackets. Here, we focus on the model for the Bethe lattice in the limit of infinite coordination number.

B. Nonequilibrium DMFT+CPA

The nonequilibrium many-body formalism can be formulated on the Keldysh contour whereby the system is evolved forward in time from an early $t = t_{\text{min}}$ to times of physical interest up to a maximum value t_{max} and then backward to the early times again [35–37]. The formalism involves several types of two-time Green's functions among which are $G^<(t, t')$ (the lesser), $G^>(t, t')$ (the greater), and $G^R(t, t')$ (the retarded) Green's functions. In the context of a system initially in equilibrium at an initial temperature $T = 1/\beta$, a vertical spur of imaginary times of length $-i\beta$ is added to the Keldysh contour resulting in the so-called Kadanoff-Baym-Keldysh contour [35,38]. In this situation, one should add to the previous types of Green's functions in the formalism, the Matsubara Green's function G^τ , and the mixed time Green's functions, where one of the times is on either one of the horizontal branches of real times, while the other is on the vertical branch of imaginary times. The solution, for a given problem, can be formulated in terms of the different Green's functions $G^<$, $G^>$, G^R , G^τ , etc. Alternatively, it can be formulated in terms of the contour-ordered Green's function $G^c(t, t')$ from which all the others can be extracted. It is this latter approach that we use in this work. The contour-ordered quantities have time ordering performed with respect to time advance along

the entire contour. Hereafter we drop the subscript c from the contour-ordered quantities for convenience.

Our solution for the above described Anderson-Hubbard model under an interaction quench is performed within the recently developed nonequilibrium DMFT+CPA formalism which builds on the equilibrium formalism [39–43] and is described extensively in Ref. [23]. Here, for the sake of completeness, we briefly summarize the algorithm. The method maps the lattice problem onto that of an impurity embedded in a self-consistently determined medium characterized by the hybridization $\Delta(t, t')$ that is consistent with that of DMFT for the clean system and with that of the disordered noninteracting system for CPA.

In practice, the algorithm consists of the following self-consistency procedure. From an initial guess of the hybridization function $\Delta(t, t')$, one obtains the noninteracting Green's function for each disorder configuration given by

$$\mathcal{G}_{V_i}(t, t') = [(i\partial_t + \mu - V_i)\delta_c - \Delta]^{-1}(t, t'). \quad (2)$$

From this, one obtains the Coulomb interaction self-energy. Here, similar to Ref. [23], we focus on the weak-to-moderate interaction and disorder strengths regime, and we use second-order perturbation theory so that the self-energy is given by

$$\Sigma_{V_i}(t, t') = -U(t)U(t')\mathcal{G}_{V_i}(t, t')^2\mathcal{G}_{V_i}(t', t). \quad (3)$$

After obtaining the self-energy for all disorder configurations, we evaluate the disorder-averaged Green's function:

$$G_{\text{ave}}(t, t') = \langle (G_{V_i}) \rangle_{\{V\}}, \quad (4)$$

where $G_{V_i}(t, t')$ is the Green's function for the disorder configuration $\{V_i\}$:

$$G_{V_i}(t, t') = [G_{V_i}^{-1} - \Sigma_{V_i}]^{-1}(t, t'). \quad (5)$$

This is followed by the evaluation of the updated hybridization function which in the present case of the Bethe lattice with infinite coordination is given by $\Delta(t, t') = t^{*2}G_{\text{ave}}(t, t')$ and the self-consistency loop is repeated starting from the calculation of the new Coulomb interaction self-energies and proceeds until convergence of the self-energy within a desired criterion. t^* is the hopping amplitude rescaled with the coordination number z so that $t_{\text{hop}} = \frac{t^*}{\sqrt{z}}$. We use $t^* = 0.25$ and, unless otherwise specified, we use the bandwidth as our energy unit and its inverse as the time unit.

C. Numerical implementation

Our implementation of the nonequilibrium DMFT+CPA follows the discrete-time construction of Refs. [11,23]. The Kadanoff-Baym-Keldysh contour is discretized into $(2N_t + N_\tau)$ time steps, where N_t is the number of time steps on each leg of the horizontal real-time branch of the contour and N_τ is the number of time steps on the vertical branch of imaginary time. The step sizes are $\Delta t = (t_{\text{max}} - t_{\text{min}})/N_t$ for real time and $\Delta \tau = \beta/N_\tau$ for imaginary time. In this paper, $t_{\text{min}} = -5$ and $t_{\text{max}} = 20$ while the initial temperature of the system is such that $\beta_{\text{initial}} = 15$.

In this context, the contour-ordered quantities such as $G(t, t')$ become square complex matrices G_{ij} of size $(2N_t + N_\tau) \times (2N_t + N_\tau)$. Convolutions of contour-ordered

quantities become matrix multiplications, and the continuous matrix inverse becomes a discrete matrix inverse. The analysis is often performed by switching from the (t, t') time coordinates to the Wigner coordinates $(T_{\text{ave}}, t_{\text{rel}})$ where T_{ave} can be viewed as the effective time of the system while frequency domain information is obtained by Fourier transforming with respect to t_{rel} . Observables calculated from the discretized contour, such as the distribution functions and the energy, are often obtained for multiple step sizes and then extrapolated to the continuum limit $\Delta t \rightarrow 0$. We use standard Lagrange interpolating polynomials to quadratic order.

III. RESULTS

The system is initially in equilibrium at temperature $T = 1/\beta$ with $\beta_{\text{initial}} = 15$. While keeping the disorder strength W constant, the interaction quench is applied at time $t = t_{\text{quench}} = 0$ with the interaction abruptly changing from an initial value $U_1 = 0$ to a final value $U = U_2$. We are interested in tracking the thermalization of the system at long times. Our analysis is guided by two fundamental quantities: the density of states and the distribution function. For a thermalized system, the former is given by the retarded Green's function, while the latter is given by the lesser Green's function. Namely,

$$\rho(\omega) = -i \text{Im} G^R(\omega)/\pi, \quad (6)$$

and according to the fluctuation dissipation theorem, for a thermalized system,

$$G^<(\omega) = -2iF(\omega)\text{Im}G^R(\omega), \quad (7)$$

where $F(\omega)$ is the distribution function. In the nonequilibrium formalism, we can track these quantities as a function of average time. Note that second-order perturbation theory, as an impurity solver for the nonequilibrium formalism, will break down beyond the very short time transient for strong interactions and disorder [23]. The following analysis is performed in the regions of parameter space where our solutions are known to be reliable.

A. Density of states

The system is initially in equilibrium with no interaction and the density of states in the absence of disorder has a semielliptic line shape centered around the Fermi energy. In the presence of disorder, this equilibrium density of states is broadened with a lower maximum. For an interacting clean system in equilibrium, the density of states gradually develops, with increasing interaction strength, two Hubbard bands and becomes gapped at a critical value of the interaction U_c . Disorder smears the features of these densities of states and delays the opening of the gap to stronger interactions [23,44].

For the system at half-filling, we know that the real part, in the time domain, of the retarded Green's function vanishes for all average times [18]. Thus, the density of states is fully defined by the imaginary part of the retarded Green's function in the time domain. For this reason, we can track the dynamics of the density of states through the imaginary part of the retarded Green's function in the time domain. Figure 1 presents the typical behavior of $G^R(T_{\text{ave}}, t_{\text{rel}})$ as a function

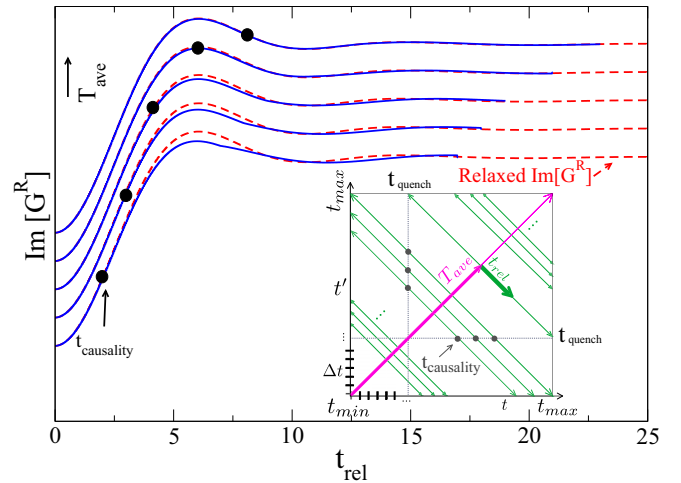


FIG. 1. Imaginary part of the retarded Green's function as a function of relative time for a range of average times, for $U_2 = 3t^*$, $W = t^*$. The long-time (relaxed) retarded Green's function is represented by the dashed red lines, and the causality time is marked for each average time with a black dot. Note that the t_{rel} at which G^R begins to diverge from its relaxed form is greater and greater with increasing T_{ave} . Inset: illustration of the relationship between $(T_{\text{ave}}, t_{\text{rel}})$ and (t, t') , with the blue vertical and horizontal lines indicating the time at which the quench occurs in t and t' and black dots indicating $t_{\text{causality}}$.

of t_{rel} for a series of T_{ave} values. Note that the relative time axis (represented by the green lines in the inset), for earlier values T_{ave} (magenta lines in the inset), has segments of time coordinates (t, t') for which one (or both) of the times is (are) before the interaction quench leading to a mixed character of the corresponding t_{rel} coordinates. The blue lines in the main figure correspond to successive T_{ave} values after the quench, while the dashed red line corresponds to an average time value after the quench for which all t_{rel} involves both t and t' that have the new interaction strength U_2 . The black circles correspond to the causality time beyond which t_{rel} has mixed character. One can see on this figure that the solid blue curves overlap with the dashed red curve up to the causality time and that the retarded Green's function is only constrained by causality. So, the density of states is immediately established after the quench. The relaxation of the system can thus be tracked through the distribution function.

B. Distribution function $F(\omega)$

In the present study, we are interested in the thermalization of the system after it has undergone its early transient following the quench. Figure 2 shows, for different disorder strengths and for $U_2 = 2t^*$, the evolution in time of the kinetic, potential, and total energies of the system evaluated following Refs. [23,45]. This relaxation of the kinetic, potential, and total energy was previously examined for various values of the interaction and disorder strengths in Ref. [23]. We observed that for a quench from a noninteracting system to a weakly interacting system, the long-time kinetic energy indeed increases with disorder strength, but as the final interaction strength is increased, this trend is reversed and the

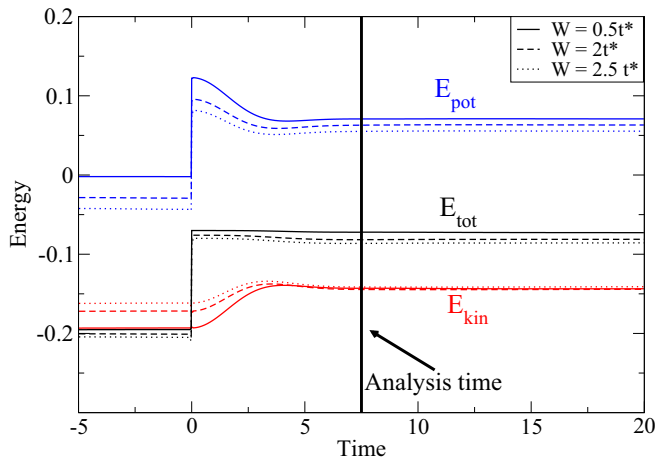


FIG. 2. Extrapolated potential, kinetic, and total energies for $U_2 = 2t^*$. The vertical black line shows the time at which we evaluate the relaxed distribution function. This time is well after the relaxation of the system.

kinetic energy decreases with increasing disorder strengths for moderate final interaction strengths. During the quench, energy is added to the system entirely through the abrupt increase of the potential energy. Thus, after the quench, in the short-time transient, as the system relaxes towards its steady state, the kinetic energy increases with time while the potential energy decreases as the system evolves towards its steady state.

The quench is performed at time $t = 0$. After an initial nontrivial response to the quench, the observables settle into a constant value for the remaining duration of the simulation. The vertical black line indicates the time $t = 7.5$ at which the long-time analysis is performed. The kinetic energy in these calculations is negative, stemming from the convention of having a minus sign in front of the hopping amplitude in the Hubbard model and in other similar tight-binding model Hamiltonians (see Ref. [27]). This minus sign accounts for the basic quantum-mechanical principle that a particle with a state extended over a larger spatial volume will have a lower energy than if it were localized. Thus, the negative sign of the kinetic energy reflects the energetically favorable electron delocalization.

Given that the density of states is established immediately after the quench and is only constrained by causality, this analysis time is chosen so as to allow a range of t_{rel} values that enables a reliable Fourier transform. To obtain the distribution function, we will use the fluctuation-dissipation theorem as expressed by Eq. (7). To this end, we first Fourier transform the lesser and retarded Green's functions $G^{R/<}(T_{\text{ave}}, t_{\text{rel}})$ in relative time to yield $G^{R/<}(T_{\text{ave}}, \omega)$. The result of this operation is illustrated for $U_2 = 2t^*$ and $W = 2t^*$ in Fig. 3. To avoid numerical instabilities, the distribution function is only evaluated in a frequency range around $\omega = 0$ for which both $G^R(T_{\text{ave}}, \omega)$ and $G^<(T_{\text{ave}}, \omega)$ remain finite as illustrated by the shaded box in Fig. 3.

Figures 4 and 5 show the extracted distribution function for $U_2 = 3t^*$ and $W = t^*$ for different average times. One can readily observe that following the interaction quench at

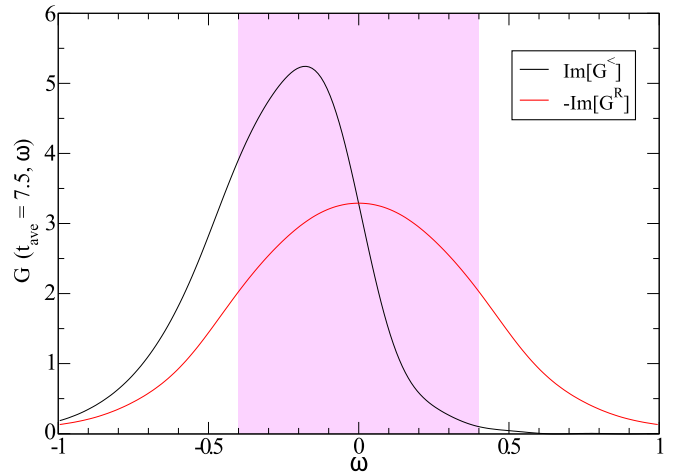


FIG. 3. Imaginary parts of lesser and retarded Green's functions as a function of frequency for $U_2 = 2t^*$, $W = 2t^*$ at the analysis time. The shaded box shows the region over which we evaluate the distribution function $F(\omega) = -\text{Im}[G^<]/(2\text{Im}[G^R])$. Outside of this region, the ratio is prone to numerical instabilities due to the Gibbs phenomenon in the frequency data obtained and to the division by small numbers.

time $t = 0$, the distribution function initially changes in a highly nontrivial way and may in fact clearly correspond to a nonthermal system (Fig. 4). However, around our analysis time, corresponding to $T_{\text{ave}} = 7.5$, the distribution function is seen to change very little for different values of the average time and the different curves essentially overlap (Fig. 5). For this reason, the system can be assumed to have settled into its long-time state at time $T_{\text{ave}} = 7.5$. It is in this regime that we evaluate a long-time effective temperature of the system after the quench.

C. Effective temperature

The effective temperature is obtained by fitting a Fermi-Dirac distribution function $[F(\omega) = 1/[1 + \exp(\beta\omega)]]$ with β

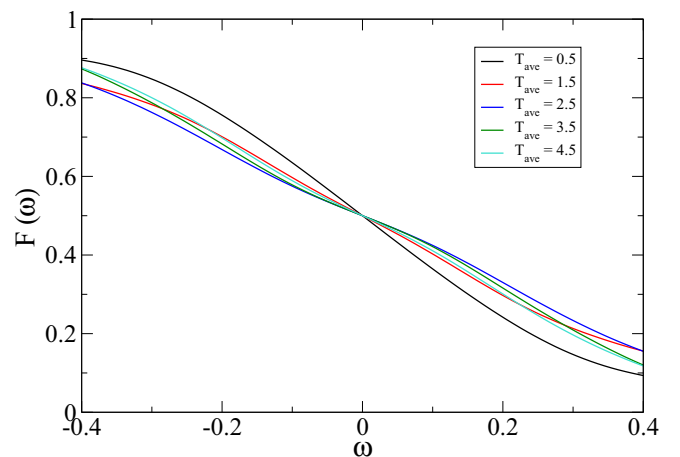


FIG. 4. Relaxation of $F(\omega)$ at $U_2 = 3t^*$, $W = t^*$ soon after the quench, but before thermalization, demonstrating the nonthermal form of the distribution function at the early stages of the relaxation.

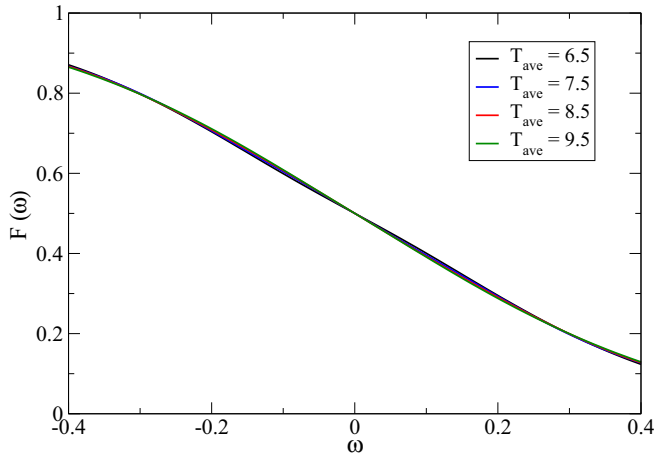


FIG. 5. Postrelaxation $F(\omega)$ for times slightly before and slightly after our analysis time for $U_2 = 3t^*$, $W = t^*$, demonstrating that the distribution function changes minimally around this analysis time at which we evaluate the relaxed $F(\omega)$.

as a free parameter] to the extracted distribution function over a frequency window around $\omega = 0$ as illustrated in Fig. 6. As indicated above, after the quench but before relaxation, the distribution function can take nonthermal forms (Fig. 4). Consequently, an effective temperature cannot be traced over the entire time evolution of the system. However, this procedure is well defined for the chosen analysis time for the long-time behavior.

Figure 7 shows the long-time effective temperature of the system as a function of the final interaction strength U_2 with different solid lines corresponding to different values of the disorder strength W . The inset shows the same data but

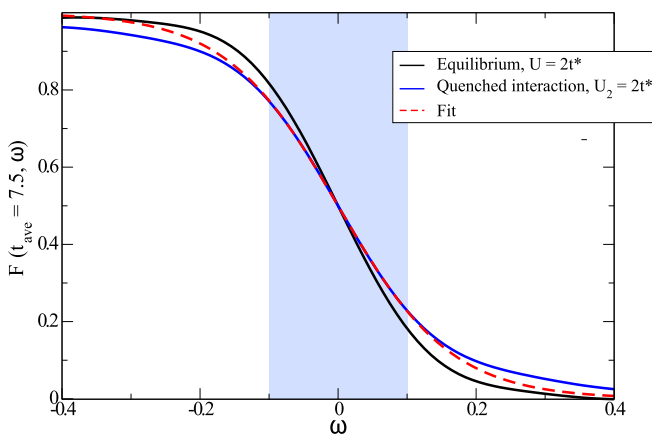


FIG. 6. Distribution function for the equilibrium system with $U = 2t^*$, $W = 2t^*$, $\beta = 15$, and after relaxation for the quenched system with $U_2 = 2t^*$, $W = 2t^*$, $\beta_{\text{initial}} = 15$. The dashed line shows the fit to the quenched system distribution function after the transient. The shaded box indicates the region over which the fit is performed. Here we fit the Fermi function, $F_{\text{Fit}}(\omega) = 1/[1 + \exp(\beta\omega)]$ with β as a free parameter, to the calculated $F(\omega)$, and this allows us to extract an effective temperature.

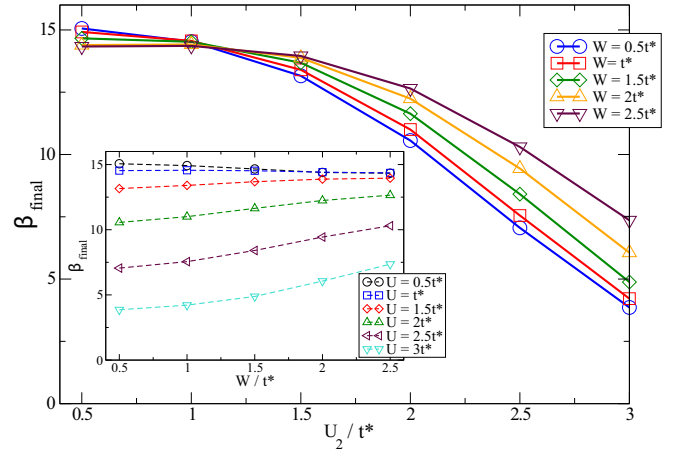


FIG. 7. Inverse effective temperature as a function of the final interaction strength for different disorder strengths. The system is initially at a temperature such that $\beta_{\text{initial}} = 15$. Inset: Effective inverse temperature β as a function of the disorder strength for different interaction strengths. Increased disorder strength for moderate interaction strengths leads to a lower long-time temperature.

with the disorder strength on the x axis and different dashed lines corresponding to different values of the final interaction strength. The figures show the significant dependence of the final inverse temperature on disorder strength. For weak U_2 values, increased disorder strength leads to a small increase in the long-time temperature. However, as the interaction strength U_2 is increased, we observe that increasing the disorder strength leads to lower long-time effective temperatures. This shows that under an interaction quench, the long-time temperature can vary over a broad range of values depending on the disorder strength, with increased disorder strength leading to a lower final temperature.

IV. CONCLUSION

We have analyzed the relaxation of a disordered interacting system after an interaction quench where, with the disorder strength held constant, the interaction strength is abruptly switched from zero to a finite value U_2 at which it is subsequently kept. We have used the recently developed nonequilibrium DMFT+CPA formalism that maps the lattice problem onto an effective mean field that is equivalent to that of the DMFT for the clean system and to that of the CPA for the disordered noninteracting system. By extracting the distribution function from the Green's function using the fluctuation-dissipation theorem, we showed that while the early transient does not follow the fluctuation dissipation theorem, at longer times, the system settles into a thermal state at a constant temperature. This long-time temperature is lowered by increased disorder strengths at moderate values of the interaction. Altogether our studies demonstrate that after the interaction quench, disorder can tune the long-time temperature of the system over a broad range of values. The identified effects of disorder on the densities of states, on the nonequilibrium distribution functions, and on the

thermalization dynamics of correlated systems away from equilibrium, will be an important factor to consider in the analysis of time-resolved spectroscopy experiments. The application of the nonequilibrium DMFT+CPA approach to these experiments will be the subject of future studies.

ACKNOWLEDGMENTS

H.F.F. is supported by the National Science Foundation under Grant No. PHY-2014023. H.T. has been supported by NSF Grant No. DMR-1944974.

-
- [1] J. M. Deutsch, *Phys. Rev. A* **43**, 2046 (1991).
 [2] M. Srednicki, *Phys. Rev. E* **50**, 888 (1994).
 [3] M. Rigol, V. Dunjko, and M. Olshanii, *Nature (London)* **452**, 854 (2008).
 [4] L. Perfetti, P. A. Loukakos, M. Lisowski, U. Bovensiepen, H. Berger, S. Biermann, P. S. Cornaglia, A. Georges, and M. Wolf, *Phys. Rev. Lett.* **97**, 067402 (2006).
 [5] L. Perfetti, P. A. Loukakos, M. Lisowski, U. Bovensiepen, H. Eisaki, and M. Wolf, *Phys. Rev. Lett.* **99**, 197001 (2007).
 [6] I. Bloch, J. Dalibard, and W. Zwerger, *Rev. Mod. Phys.* **80**, 885 (2008).
 [7] M. Greiner, O. Mandel, T. Esslinger, T. W. Hänsch, and I. Bloch, *Nature (London)* **415**, 39 (2002).
 [8] I. Bloch, *Nat. Phys.* **1**, 23 (2005).
 [9] W. S. Bakr, J. I. Gillen, A. Peng, S. Fölling, and M. Greiner, *Nature (London)* **462**, 74 (2009).
 [10] J. K. Freericks, V. M. Turkowski, and V. Zlatić, *Phys. Rev. Lett.* **97**, 266408 (2006).
 [11] J. K. Freericks, *Phys. Rev. B* **77**, 075109 (2008).
 [12] H. Aoki, N. Tsuji, M. Eckstein, M. Kollar, T. Oka, and P. Werner, *Rev. Mod. Phys.* **86**, 779 (2014).
 [13] R. Nandkishore and D. A. Huse, *Annu. Rev. Condens. Matter Phys.* **6**, 15 (2015).
 [14] S. S. Kondov, W. R. McGehee, W. Xu, and B. DeMarco, *Phys. Rev. Lett.* **114**, 083002 (2015).
 [15] D. A. Abanin, E. Altman, I. Bloch, and M. Serbyn, *Rev. Mod. Phys.* **91**, 021001 (2019).
 [16] M. Eckstein, M. Kollar, and P. Werner, *Phys. Rev. Lett.* **103**, 056403 (2009).
 [17] M. Eckstein and M. Kollar, *Phys. Rev. Lett.* **100**, 120404 (2008).
 [18] H. F. Fotsó, K. Mielson, and J. K. Freericks, *Sci. Rep.* **4**, 4699 (2014).
 [19] H. F. Fotsó and J. K. Freericks, *Front. Phys.* **8**, 324 (2020).
 [20] J. K. Freericks, *Phys. Rev. B* **70**, 195342 (2004).
 [21] M. Eckstein and P. Werner, *Phys. Rev. B* **84**, 035122 (2011).
 [22] B. Moritz, A. F. Kemper, M. Sentef, T. P. Devereaux, and J. K. Freericks, *Phys. Rev. Lett.* **111**, 077401 (2013).
 [23] E. Dohner, H. Terletska, K.-M. Tam, J. Moreno, and H. F. Fotsó, *Phys. Rev. B* **106**, 195156 (2022).
 [24] W. Metzner and D. Vollhardt, *Phys. Rev. Lett.* **62**, 324 (1989).
 [25] Y. Kuramoto, *Springer Series in Solid State Science*, edited by T. Kasuya and T. Sao (Springer, New York, 1985), Vol. 62, p. 152.
 [26] E. Müller-Hartmann, *Z. Phys. B* **74**, 507 (1989).
 [27] A. Georges, G. Kotliar, and W. Krauth, and M. J. Rozenberg, *Rev. Mod. Phys.* **68**, 13 (1996).
 [28] J. K. Freericks and V. Zlatić, *Rev. Mod. Phys.* **75**, 1333 (2003).
 [29] P. Soven, *Phys. Rev.* **156**, 809 (1967).
 [30] S. Kirkpatrick, B. Velický, and H. Ehrenreich, *Phys. Rev. B* **1**, 3250 (1970).
 [31] B. Velický, *Phys. Rev.* **184**, 614 (1969).
 [32] F. Yonezawa and K. Morigaki, *Prog. Theor. Phys. Suppl.* **53**, 1 (1973).
 [33] Y. Zhu, L. Liu, and H. Guo, *Phys. Rev. B* **88**, 205415 (2013).
 [34] A. V. Kalitsov, M. G. Chshiev, and J. P. Velev, *Phys. Rev. B* **85**, 235111 (2012).
 [35] L. V. Keldysh, *Zh. Eksp. Teor. Fiz.* **47**, 1515 (1964) [*Sov. Phys. JETP* **20**, 1018 (1965)].
 [36] G. Stefanucci and R. van Leeuwen, *Nonequilibrium Many-Body Theory of Quantum Systems: A Modern Introduction* (Cambridge University Press, Cambridge, UK, 2013).
 [37] J. Rammer, *Quantum Field Theory of Non-equilibrium States* (Cambridge University Press, Cambridge, UK, 2007).
 [38] L. P. Kadanoff and G. Baym, *Quantum Statistical Mechanics* (Benjamin, New York, 1962).
 [39] D. Semmler, K. Byczuk, and W. Hofstetter, *Phys. Rev. B* **84**, 115113 (2011).
 [40] E. Miranda and V. Dobrosavljević, Dynamical mean-field theories of correlation and disorder, in *Conductor-Insulator Quantum Phase Transitions*, edited by V. Dobrosavljevic, N. Trivedi, and J. M. Valles, Jr. (Oxford University Press, 2012), pp. 161–243.
 [41] E. Z. Kuchinskii, N. A. Kuleeva, I. A. Nekrasov, and M. V. Sadovskii, *J. Exp. Theor. Phys.* **110**, 325 (2010).
 [42] A. Weh, Y. Zhang, A. Östlin, H. Terletska, D. Bauernfeind, K.-M. Tam, H. G. Evertz, K. Byczuk, D. Vollhardt, and L. Chioncel, *Phys. Rev. B* **104**, 045127 (2021).
 [43] V. Janiš and D. Vollhardt, *Phys. Rev. B* **46**, 15712 (1992).
 [44] K. Byczuk, W. Hofstetter, and D. Vollhardt, *Int. J. Mod. Phys. B* **24**, 1727 (2010).
 [45] M. Eckstein, M. Kollar, and P. Werner, *Phys. Rev. B* **81**, 115131 (2010).